AIAA JOURNAL
Vol. 37, No. 10, October 1999

Feasibility Study of e^N Transition Prediction in Navier–Stokes Methods for Airfoils

Hans W. Stock*
DLR, German Aerospace Center, 38108 Braunschweig, Germany
and
Werner Haase†
DaimlerChrysler Aerospace AG, 81663 Munich, Germany

When Navier–Stokes methods are applied in the design process for laminar airfoils, the prediction of the transition location still represents an unresolved problem. By the acceptence of the e^N method as representing a convenient transition prediction tool, the requirements for coupling e^N to Navier–Stokes methods will be demonstrated. In particular, the possibility to determine the laminar and turbulent viscous length scales is outlined. Based on the knowledge of the viscous layer thickness, a mesh adaption procedure can be applied. The Navier–Stokes results produced using adapted meshes are shown to be identical to boundary-layer results, when the computed wall pressure from the Navier–Stokes solution is used as input for the boundary-layer calculation. For the validation of the necessary steps in the coupling procedure, the laminar airfoil DoAL3 was selected. This airfoil was measured in the Transonic Wind Tunnel Braunschweig facility at the DLR, German Aerospace Research Establishment. The limiting N factor for that wind tunnel was determined beforehand.

Nomenclature

C = chord length
c_D = drag coefficient
c_f = skin friction coefficient, $\tau_w/\frac{1}{2}\rho_\infty U_\infty^2$
c_L = lift coefficient
c_M = moment coefficient
C_p = specific heat capacity at constant pressure
c_p = pressure coefficient
E = kinetic energy parameter, $U_e^2/2H_e$
F = diagnostic function, Eq. (1)
f = nondimensional stream function, $f' = \mathrm{d}f/\mathrm{d}\eta$ equal to U/U_e
G = total enthalpy function, $2(H - H_e)/U_e^2$
H = total enthalpy, $(h + U^2)/2$
H_i = kinematic shape parameter, δ_i^*/θ_i
h = specific static enthalpy, $C_p T$
k = von Kármán constant
M = Mach number
N = N factor
Pr = Prandtl number
Re = Reynolds number based on chord and freestream conditions
S = total enthalpy function, $(H - H_e)/H_e$ equal to EG
S_w = heat transfer parameter, $(H_w - H_e)/H_e$
U = velocity component in wall parallel direction
U_τ = friction velocity, $(\tau_w/\rho_w)^{\frac{1}{2}}$
U^+ = dimensionless velocity, U/U_τ
X = coordinate in the freestream direction
Y = wall normal coordinate
y^+ = dimensionless wall distance, YU_τ/ν
α = angle of attack
β = Falkner–Skan pressure gradient parameter
δ = boundary-layer thickness
δ^* = displacement thickness, $\int_0^\delta \left(1 - \frac{\rho U}{\rho_e U_e}\right) \mathrm{d}Y$
δ_i^* = kinematic displacement thickness, $\int_0^\delta \left(1 - \frac{U}{U_e}\right) \mathrm{d}Y$
ε = constant in Eq. (2)
η = wall distance in the similarity plane
$\eta_{\max}$ = value of η for which F_{lam} is $(F_{\mathrm{lam}})_{\max}$
η_δ = value of η for which U/U_e equals 0.99
θ = momentum loss thickness, $\int_0^\delta \frac{\rho U}{\rho_e U_e}\left(1 - \frac{\rho U}{\rho_e U_e}\right) \mathrm{d}Y$
θ_i = kinematic momentum loss thickness, $\int_0^\delta \frac{U}{U_e}\left(1 - \frac{U}{U_e}\right) \mathrm{d}Y$
ν = kinematic viscosity
ρ = density
τ = shear stress
Ψ = angle between the resultant flow direction U_e at the outer edge of the boundary layer and the perturbation propagation direction

Subscripts

e = outer edge of boundary layer
lam = laminar regime
max = maximum value
ref = reference condition
w = value at the wall
∞ = freestream conditions

I. Introduction

ONE of the most challenging demands in the aerodynamics of laminar airfoils and wings is a reliable computation of boundary-layer transition. The range of existing transition prediction methods extends from simple empirical relationships through different levels of stability theories (parallel flow and linear and linear or nonlinear parabolized stability equation methods) to direct

Received 20 June 1998; revision received 10 October 1998; accepted for publication 15 March 1999.

*Senior Research Scientist, Institute of Design Aerodynamics, Lilienthalplatz 7.
†Senior Research Scientist, Flight Physics Department, Military Aircraft Division, P.O. Box 801160.

numerical simulations. The e^N method, based on linear stability theory and the parallel flow assumption, is the most frequently used method in the aircraft industry for the design of laminar wings.

In general, computational design approaches involve the application of viscous/inviscid interactive methods in conjunction with transition prediction procedures based on the e^N method.[1] In the present approach, the complete flowfield is predicted by a Navier–Stokes solver. The procedure of coupling this code to the e^N transition prediction method will be outlined.

A. Generation of Adapted Meshes

To produce reliable laminar data for the stability analysis, it will be demonstrated that the mesh for the Navier–Stokes computation has to be accurately generated. In the wall normal direction, a sufficiently large and, more importantly, a constant number of mesh points has to be embedded inside the viscous layer from the stagnation point to the airfoil trailing edge.

The viscous layer thickness in the laminar and turbulent flow regimes is not known a priori in Navier–Stokes computations. The procedure of determining the laminar boundary-layer thickness from Navier–Stokes data will be presented. The length scales for the turbulent viscous layer are evaluated using the approach given in Ref. 2. The benefits of knowing the viscous layer thickness are twofold. First, a mesh adaption based on the viscous flow data is feasible. Second, a length scale, i.e., the displacement thickness, of the laminar boundary layer can be described for the stability analysis.

B. Validation of the Navier–Stokes Results

The laminar viscous flow results of the Navier–Stokes calculation are validated by comparison to boundary-layer results. These are generated by using the pressure distribution obtained from the Navier–Stokes calculation as input to a finite difference laminar boundary-layer code. Similarly, the stability data computed for the Navier–Stokes data are then compared with those results calculated on the basis of the boundary-layer data.

C. Coupling of the Navier–Stokes Code to the e^N Method

Three procedures are described: 1) coupling the Navier–Stokes approach directly to the stability method, 2) using the boundary-layer method as an intermediate tool without Navier–Stokes mesh adaptation to reduce the computational effort, and 3) replacing the stability method by a database method. By use of the third procedure, a further considerable reduction in the engineering effort is achievable. Only this approach offers the chance to completely automate the iterative coupled application of the Navier–Stokes, the boundary-layer, and the database methods.

D. Computational Methods Applied

The Reynolds averaged Navier–Stokes equations, describing two-dimensional, unsteady, compressible flows in conservation form, are solved by means of a finite volume approach using a Runge–Kutta time-stepping method with multigrid acceleration.[3] In the turbulent part of the viscous layer, the Johnson–King turbulence model is applied in its original form.[4]

The boundary-layer method for laminar, compressible flows on swept, tapered wings[5] is a finite difference method with second-order accuracy in the marching direction and fourth-order accuracy in the wall normal direction; hence, it is free of any numerical viscosity, in contrast to the Navier–Stokes method.

The stability method[6] solves the three-dimensional, compressible Orr–Sommerfeld stability equations using a finite difference scheme.

II. Evaluation of the Viscous Length Scales

In the past, the problem of determining the viscous length scales in Navier–Stokes computations has been treated only partially successfully for turbulent flows. However, for laminar flows, no adequate procedure is known. Most techniques for determining the outer edge of the viscous layer start in the inviscid flowfield and approach the viscous layer using a suitable criterion. In contrast, the length scales in the present paper are calculated by investigating the viscous layer starting at the wall; thus, the detection criterion is found inside the viscous layer.

It is shown in Ref. 2 that the turbulent length scales can be evaluated from Navier–Stokes data using the diagnostic function F:

$$F = Y^a \left[\frac{\mathrm{d}U}{\mathrm{d}Y}\right]^b \tag{1}$$

resulting in the boundary-layer thickness

$$\delta = \varepsilon Y_{\max} \tag{2}$$

where $Y_{\max}$ is the wall distance, for which $F = F_{\max}$. The assumption, that Coles[7] velocity profiles describe the turbulent boundary-layer flow sufficiently accurately allows one to compute the values for a, b, and ε such that

$$F_{\text{turb}} = Y\left[\frac{\mathrm{d}U}{\mathrm{d}Y}\right] \qquad (a = b = 1) \tag{3}$$

$$\delta_{\text{turb}} = 1.936 Y_{\max} \qquad (\varepsilon = 1.936) \tag{4}$$

The same diagnostic function F [Eq. (1)] may now be used to compute the boundary-layer thickness for laminar flows. For the determination of the constants a, b, and ε, the quasi-similar solutions for compressible, laminar boundary layers including heat transfer effects[8] are applied. The following equations are solved:

$$f''' + ff'' + \beta(1 - f'^2 + EG) = 0 \tag{5}$$

$$G_1'' + PrfG_1' - 2Pr\beta(1 - E)f'G_1 - 2(1 - Pr)(f'f'')' = 0 \tag{6}$$

$$G_2'' + PrfG_2' = 0 \tag{7}$$

$$G(\eta) = EG_1(\eta) + G_2(\eta) \tag{8}$$

with the boundary conditions at $\eta = 0$

$$f = f' = 0, \qquad G_1' = 0, \qquad G_2 = G_{2w}$$

and with the boundary conditions at $\eta \to \infty$

$$f' \to 1, \qquad G_1 \to 0, \qquad G_2 \to 0$$

and $Pr = 0.72$.

Quasi-similar solutions are established for different Mach numbers and pressure gradients that cover the whole range from highly accelerated up to reversed flow situations, including adiabatic, cooling, and heating cases. Figure 1 shows velocity profiles in adiabatic

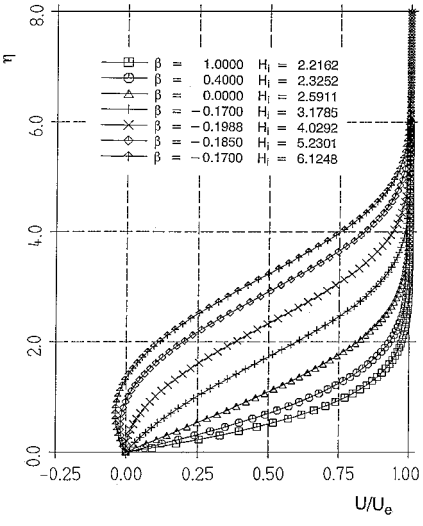

Fig. 1 Laminar velocity profiles generated by quasi-similar solutions of the boundary layer for different values of the pressure gradient parameter β in incompressible flow.

flows for different values of the pressure gradient parameters β in incompressible flow, including reversed flow data.

Through numerical experimentation, the values of a and b are determined that produce a nearly unique value for ε in all considered cases resulting in

$$F_{\text{lam}} = Y^{3.9}\left[\frac{dU}{dY}\right] \qquad (a = 3.9 \text{ and } b = 1) \tag{9}$$

$$\delta_{\text{lam}} = 1.294 Y_{\max} \qquad (\varepsilon = 1.294) \tag{10}$$

Based on the velocity profiles (Fig. 1), the diagnostic function F_{lam} and the ratio $(F/F_{\max})_{\text{lam}}$ are given in Fig. 2 vs η and η/η_δ, respectively. As can be seen, the maximum of F_{lam} occurs at a constant value of η/η_δ. The quantity is $\eta_{\max}/\eta_\delta$ is shown in Fig. 3 as a function of the shape parameter H_i for different Mach numbers and adiabatic, cooling, and heating conditions. Small values of H_i represent accelerated flows and large values highly retarded flows, including separation. One can easily recognize that the value of $\eta_{\max}/\eta_\delta$ is nearly constant for all flow situations considered. Finally, in Fig. 4, the exact value of η_δ is compared to the approximated value for η_δ, namely, $\varepsilon\eta_{\max}$. The agreement is fairly tolerable, considering the variations in Mach number, pressure gradient, and heat transfer rate.

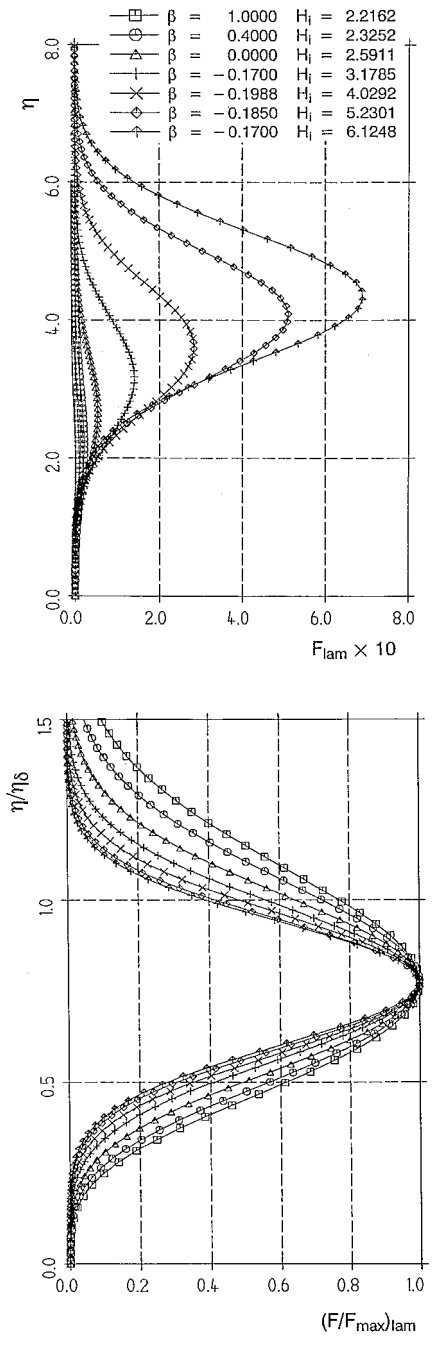

Fig. 2 Diagnostic function F_{lam} in wall normal direction.

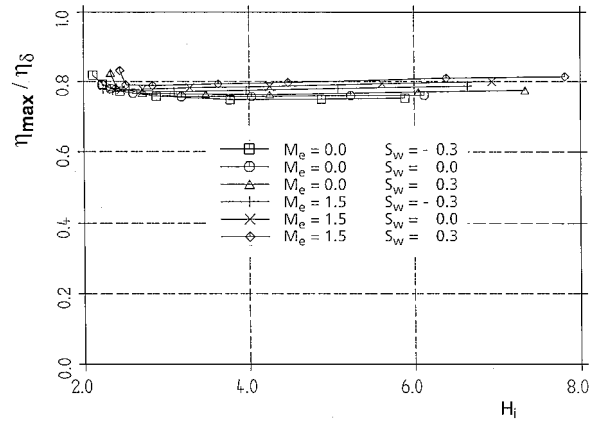

Fig. 3 Quantity $\eta_{\max}/\eta_\delta$ as a function of the shape parameter H_i.

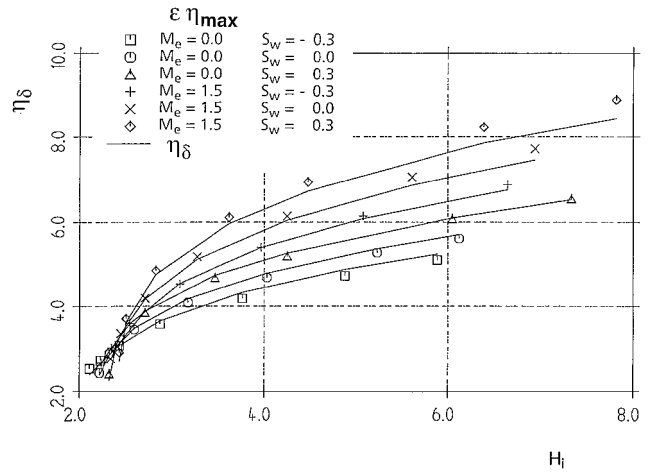

Fig. 4 Comparison of η_δ and the value $\varepsilon\eta_{\max}$ depending on the shape parameter H_i.

III. Results

The laminar airfoil DoAL3, developed at Dornier, is used for the present study. The lift and drag polars, computed by the Navier–Stokes method, are shown in Fig. 5. The measurements were performed in the Transonic Wind Tunnel Braunschweig (TWB) facility at the DLR, German Aerospace Research Establishment.[9] The measured data are compared to calculations for the initial and the adapted meshes. Transition is fixed on the upper and lower surface at the laminar separation point, which represents the most downstream position of laminar flow, if laminar separation bubbles are not considered. The maximum lift is predicted reasonably well, whereas the value of $dc_L/d\alpha$ is clearly overpredicted. This is because the tunnel walls of the TWB are slotted, and the porosity appears to be too high.[10] The drag, especially the minimum drag, is predicted well, except the extent of the laminar bucket is far overpredicted. The reason is that transition is set to the laminar boundary-layer separation point, which overestimates the extent of laminar flow on the airfoil in that wind tunnel.

The results for lift and drag obtained with the initial and the adapted meshes are almost undiscernible. It is well known that in weak interacting flows changes in the near wall mesh in Navier–Stokes methods do not significantly affect the pressure distribution. The agreement of the corresponding pressure distributions computed for an angle of attack of $\alpha = 2$ deg is documented in Fig. 6.

Further investigations are now concentrated on a single angle of attack, which lies outside the experimentally observed laminar

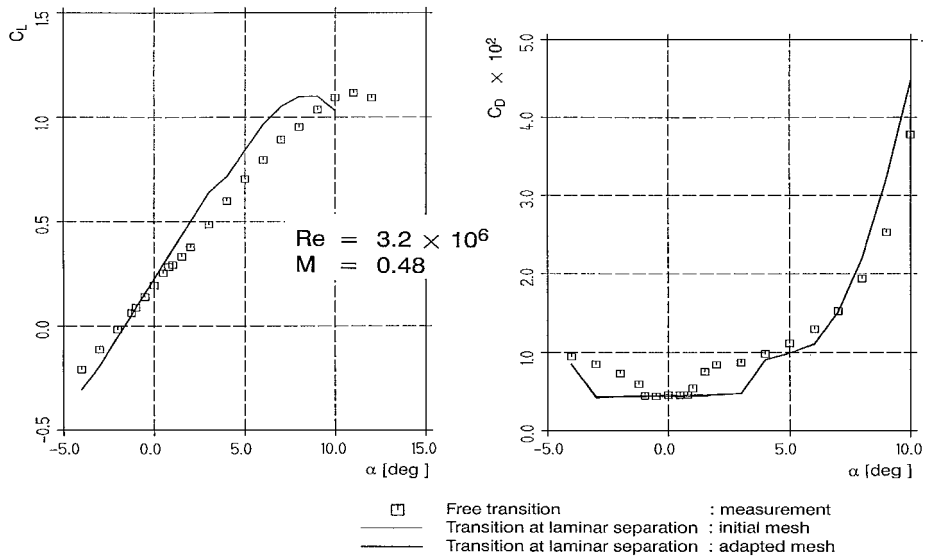

Fig. 5 Lift and drag polar for the DoAL3 airfoil.

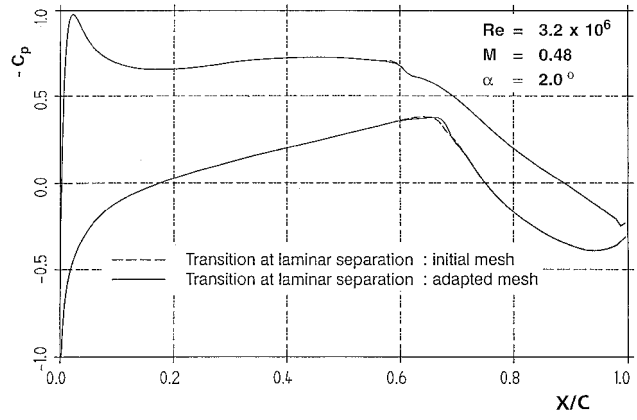

Fig. 6 Pressure distribution computed with the initial and the adapted mesh.

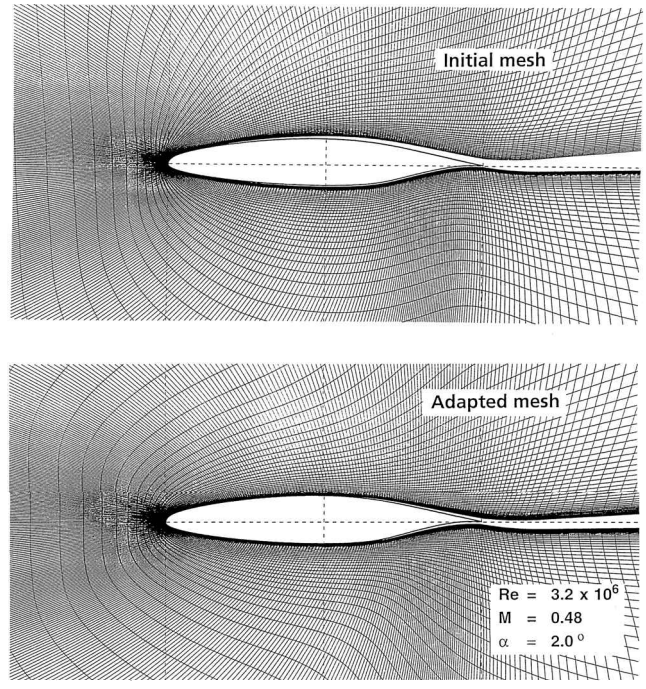

Fig. 7 Closeup view of the initial and adapted mesh.

bucket, but inside the computed laminar bucket. For the current study, an angle of attack of $\alpha = 2$ deg is chosen.

A. Coupling Procedure

The Navier–Stokes computation is started using the initial mesh with transition set just before the point of laminar separation. This location is chosen because it represents the most downstream position of laminar flow, ignoring laminar separation bubbles. Furthermore, it guarantees that the transition location can only move upstream.

After that initial computation, mesh adaption with respect to the viscous layer is applied. The calculation then continues, and the viscous layer data are analyzed with the stability method. The X/C transition location is determined, where the envelope of the N curves achieves the limiting N factor. The new transition locations are transferred in a slightly underrelaxed manner on both the lower and upper surfaces. The Navier–Stokes computation is then repeated, and a newly adapted mesh is produced. This process is repeated until a converged solution is found. For the current cases two iterations were sufficient.

B. Initial and Adapted Meshes

Four mesh levels are employed for the multigrid procedure with 512×128 mesh volumes in the finest grid. The initial and the adapted meshes are shown in Fig. 7. The empty space in between the airfoil contour and the first mesh line actually contains 70 additional mesh lines in the wall normal direction. The major differences, of course, occur in the rear part of the airfoil, with the empty space in the adapted mesh closely matching the boundary-layer thickness on lower and upper surface, respectively. For additional clarity, the initial and the adapted meshes on the upper surface of the airfoil are shown in Fig. 8. In Fig. 8, only the mesh lines Y/C (i, j = const, with j representing the wall normal direction) are shown, together with the nondimensional value of the boundary-layer thickness δ/C, evaluated from Eqs. (4) and (10).

It may be clearly seen that the adapted mesh is aligned with the boundary-layer thickness, i.e., the contour of δ/C is almost identical to a mesh line Y/C. In between the airfoil and the wall distance δ, a constant number of mesh lines is embedded at every station X/C on the upper and lower surface of the airfoil. Conventionally, 60–65 mesh points are used inside the viscous layer. Furthermore, the adapted mesh takes into account both the laminar and the turbulent flow regimes, with transition fixed at the point of laminar boundary-layer separation. In the current case, this is at $X/C \approx 0.6$ on the upper surface.

Figure 9 describes the structure of the mesh inside the viscous layer. Each value of Y is divided by a reference value Y_{ref}, where

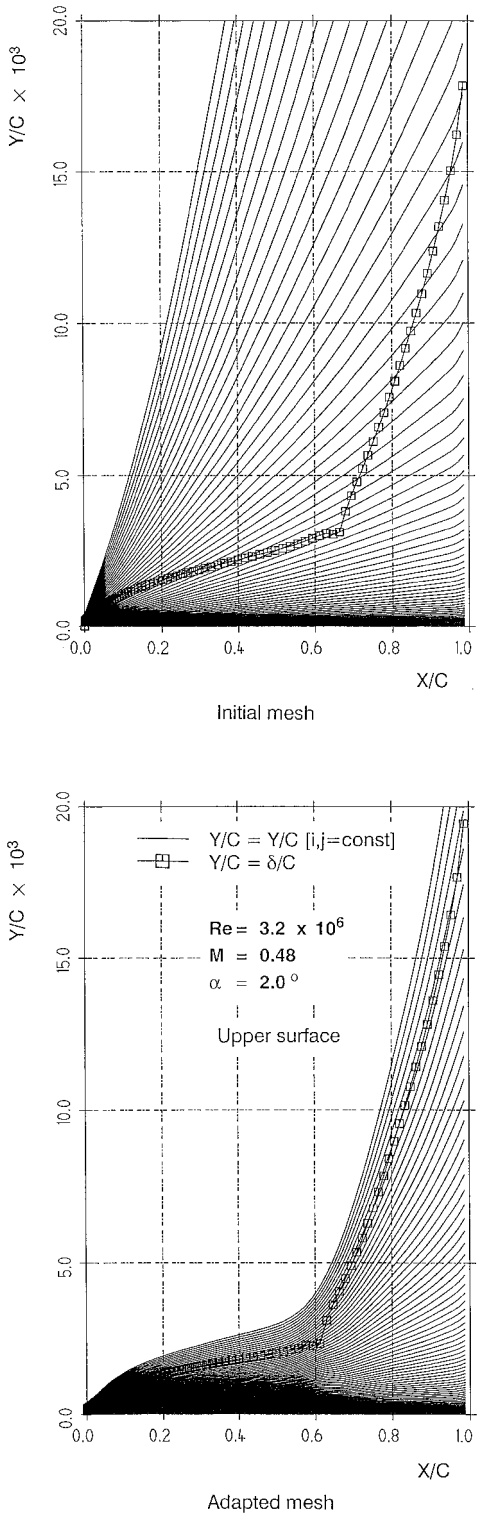

Fig. 8 Near-wall mesh lines on the upper surface of the airfoil.

Y_{ref} is the mesh line Y for $j = 70$. In the laminar flow regime, $0 \leq X/C \leq 0.6$, the mesh in wall normal direction exhibits a near unity stretching factor producing a nearly equidistant mesh; whereas in the turbulent regime a larger stretching factor is applied, resulting in a near wall clustering of mesh lines. The different stretching is caused by the approximate adaption technique, which relates the wall normal spacing of the viscous mesh to the curvature of the velocity profiles in the laminar and turbulent flow regimes, respectively. Furthermore, care is taken so that the resulting value of y^+ for the first mesh line adjacent to the wall is not larger than one. The mesh in between the fully laminar and fully turbulent flow regime is generated by applying a suitable spline function.

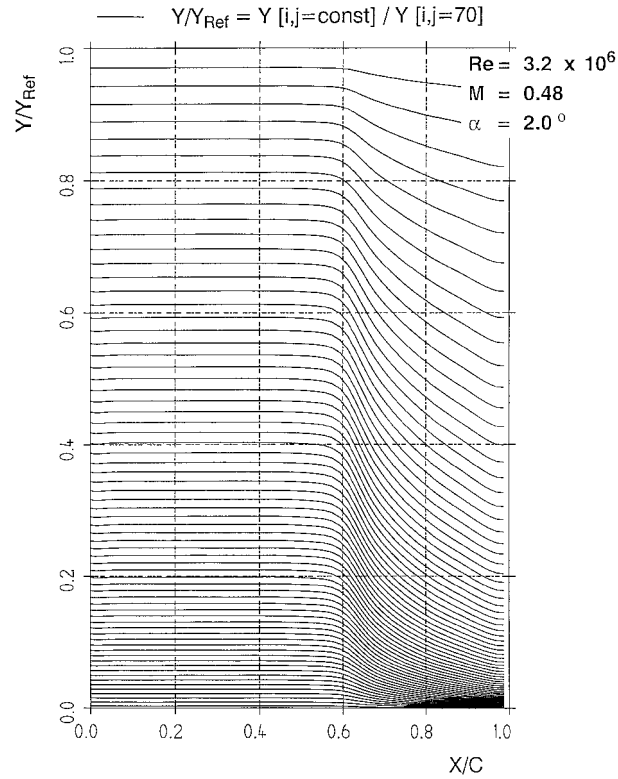

Fig. 9 Adapted mesh structure on the upper side of the airfoil.

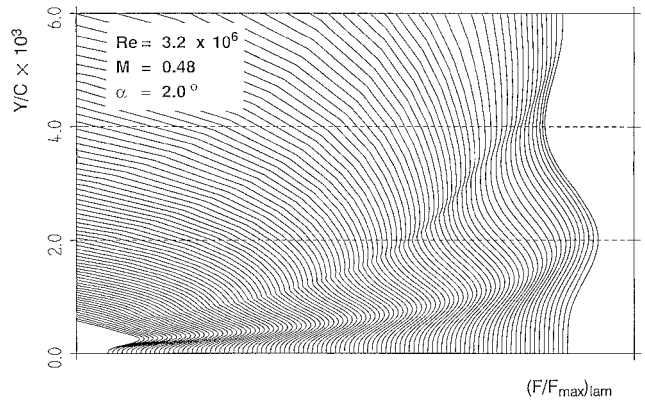

Fig. 10 Diagnostic function F_{lam} on the upper side of the airfoil computed with the adapted mesh.

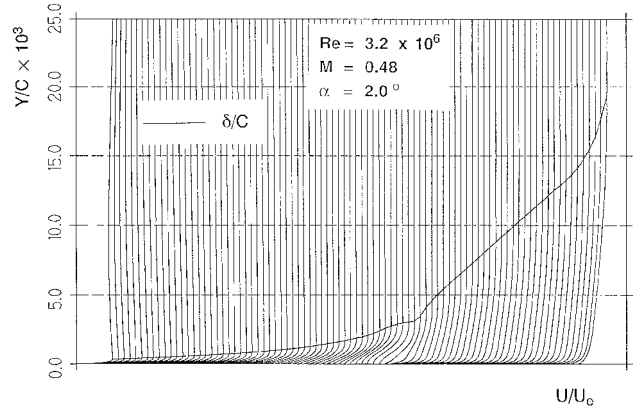

Fig. 11 Velocity ratio U/U_e, and boundary-layer thickness δ on the upper side of the airfoil computed with the adapted mesh.

C. Grid Independence

The grid dependence of the Navier–Stokes results, computed in the adapted mesh, is documented in Table 1 for an angle of attack of $\alpha = 2$ deg. The values of the drag, lift, and moment coefficients are used as indicators. As can be seen, the results can be considered as grid independent starting at the mesh level 512×128.

D. Viscous Layer Data

Figure 10 presents the diagnostic function $(F/F_{\max})_{\text{lam}}$ on the upper surface for the adapted mesh computation. The first maximum clearly defines the position $Y_{\max}$, which delivers an estimate of the viscous layer thickness [Eq. (10)]. The corresponding velocity profiles U/U_e are shown in Fig. 11 together with the δ/C contour for both the laminar and turbulent flow regions, where U_e is the value of U at the wall distance δ.

Thus far, the inviscid flow results computed by the Navier–Stokes method do not appear to be influenced by the mesh adaption, as documented by the matching of pressures and forces. In contrast, apart from the skin friction, the viscous results clearly differ. To quantify the Navier–Stokes viscous results, they will be compared to boundary-layer results, which are believed to be of higher accuracy.

The momentum loss thickness θ and the kinematic value of the shape parameter H_i are plotted in Fig. 12 vs X/C on the upper surface of the airfoil for the initial mesh computation. The Navier–Stokes results exhibit considerable overall discrepancies compared to the boundary-layer results. In particular, the values for H_i are clearly underpredicted, leading to incorrect stability data when applying the incompressible analysis.[6] The N curves evaluated for Tollmien–Schlichting waves with the propagation direction $\Psi = 0$ for unstable frequencies between 3 and 35 kHz are shown in Fig. 13. For the same pressure distribution, the Navier–Stokes viscous layer data are clearly less unstable than the boundary-layer data, and according to limiting N factors of 5–7, transition will not be predicted at all.

For the adapted mesh calculations, Figs. 14 and 15 give the corresponding information. Here, the agreement is almost perfect, documenting that laminar Navier–Stokes data, including the computation of the second derivatives of the U velocity profiles, can be produced accurately, i.e., with boundary-layer quality; that is if and only if the viscous flowfield resolution is adequate.

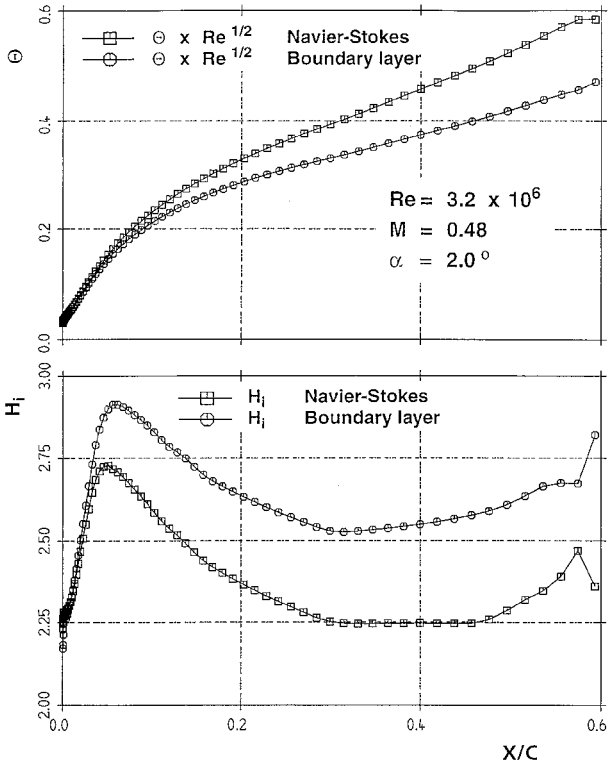

Fig. 12 Momentum loss thickness and shape parameter on the upper side of the airfoil computed with the initial mesh.

E. Limiting N Factor

Köster and Müller[11] calibrated the limiting N factor for the TWB facility, DLR, German Aerospace Research Establishment, applying incompressible analysis[6] for the e^N method. They tested several two-dimensional airfoils, recording the pressure distribution

Table 1 Navier–Stokes results grid dependence

Grid points	$c_D \times 10^2$	c_L	$c_M \times 10$
64×16	0.20153	0.43552	−0.63063
128×32	0.73753	0.51083	−0.66132
256×64	0.49365	0.50338	−0.62948
512×128	0.45595	0.49928	−0.62313
1024×256	0.45290	0.49875	−0.62191

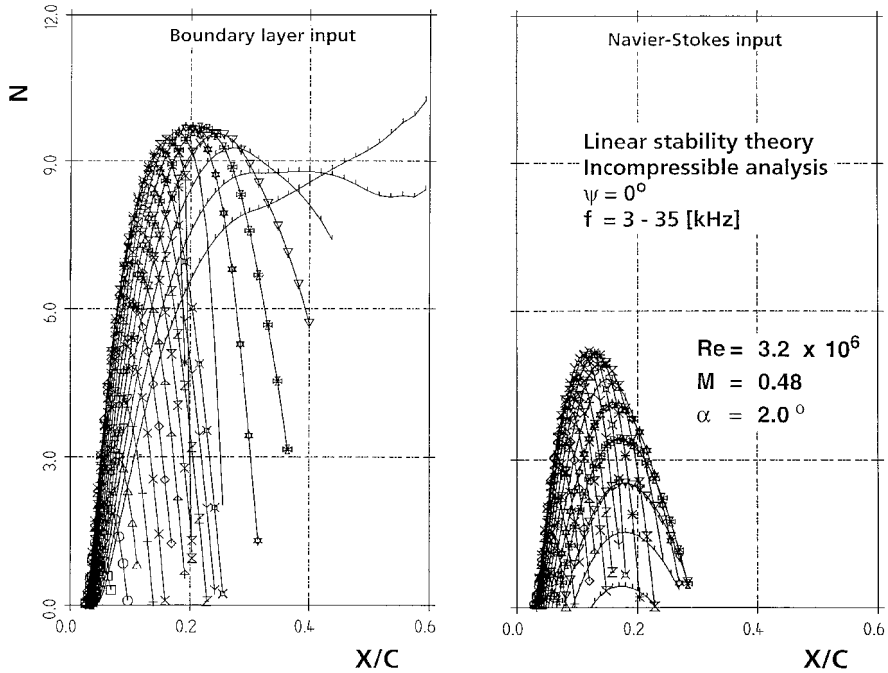

Fig. 13 N curves for unstable waves on the upper side of the airfoil computed for the initial mesh data.

and the transition location. Boundary-layer data have been evaluated for the different test cases using the measured pressure distribution as input. Subsequently, stability data were computed, and the value on the envelope of the N curves at the position of the experimentally observed transition location was determined. This N value represents the limiting N factor for the TWB wind tunnel. It is shown in Ref. 11 that the limiting N factor ranges from 5 to 7, depending slightly on the Mach number, but clearly on the Reynolds number. Based on this information, the value of $N = 6$ is used for the actual case.

F. Length of the Transitional Viscous Layer

To limit the scope of the present study, no further investigation is undertaken to clarify the influence of the length of the transition zone on the computational results. At the transition location, the turbulence model is switched on without any intermittency considerations (point transition). Figure 16 shows the upper side pressure distribution and the displacement thickness for the two cases, where point transition is imposed at the laminar separation point and at $X/C = 0.08$, which represents the final iterated transition location for the limiting N factor, $N = 6$. In both pressure distributions,

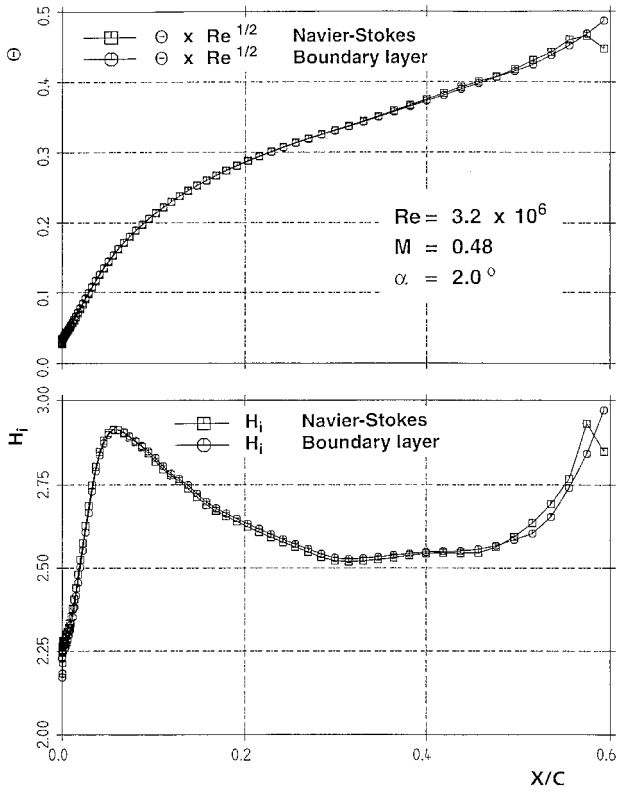

Fig. 14 Momentum loss thickness and shape parameter on the upper side of the airfoil computed with the adapted mesh.

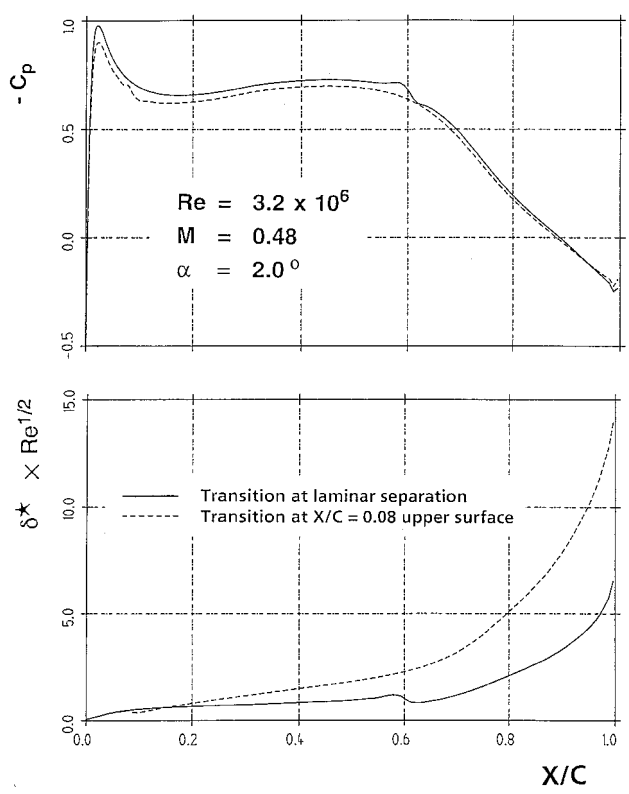

Fig. 16 Pressure and displacement thickness on the upper side of the airfoil computed with the adapted mesh.

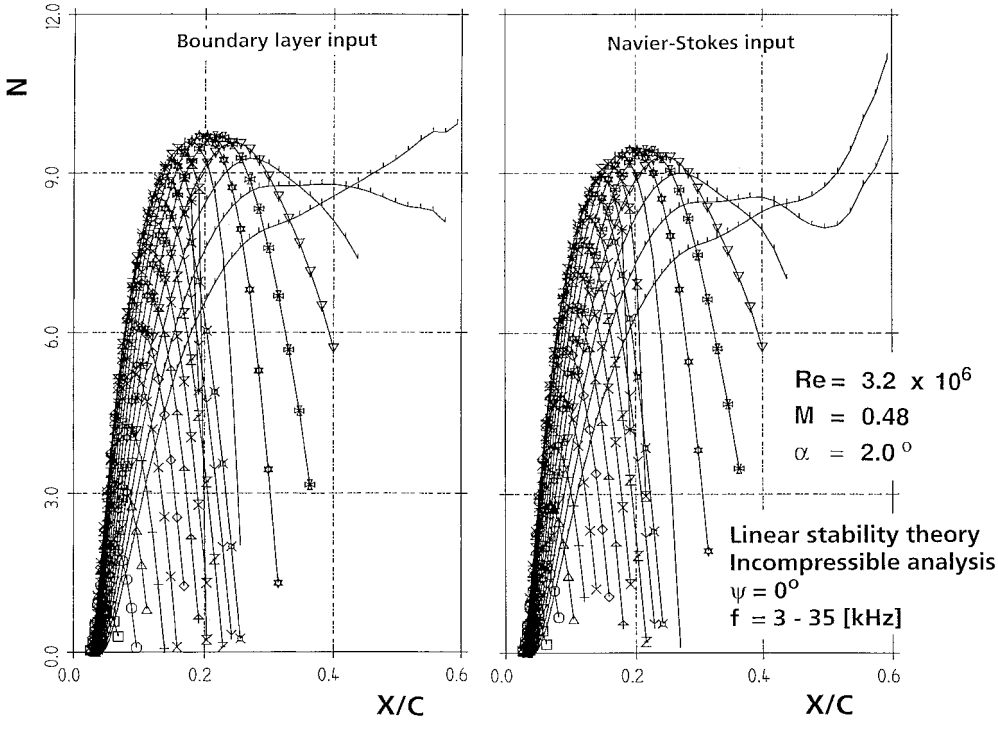

Fig. 15 N curves for unstable waves on the upper side of the airfoil computed for the adapted mesh data.

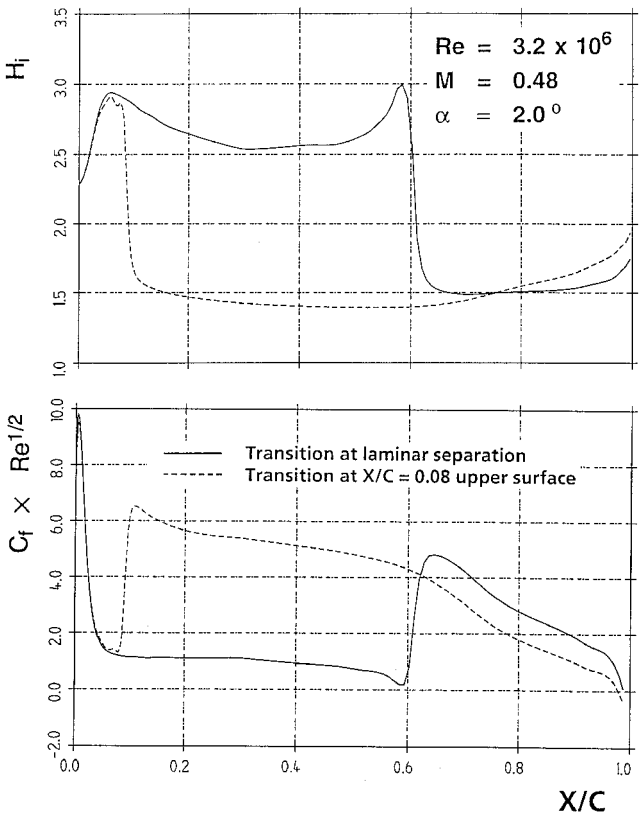

Fig. 17 Shape parameter and skin friction on the upper side of the airfoil computed with the adapted mesh.

perturbations are visible at the transition location. This is because the transition from fully laminar to fully turbulent boundary-layer flow is too abrupt, producing a relatively sharp reduction in the displacement thickness downstream of transition.

For the same flow conditions, the skin-friction coefficient and the kinematic value of the shape parameter H_i are given in Fig. 17. Although point transition is applied, one can see that a small transitional zone forms. For a variety of X/C stations, the computed velocity profiles U/U_e (Fig. 18) are provided in the interesting region from $X/C = 0.074$ up to $X/C = 0.13$ for the case that transition is predicted; the stations from $X/C = 0.074$ up to $X/C = 0.092$ represent each computational X/C station in the finest mesh. The velocity profiles are plotted against Y/C (Fig. 18a), illustrating the boundary-layer growth. In addition, the velocity profiles are presented in conventional boundary-layer form (Fig. 18b) and in nondimensional form $U^+ = f(y^+)$ (Fig. 18c). The law of the wall

$$U^+ = 1/k\,\ell_n y^+ + \text{const} \tag{11}$$

is shown for comparison as a broken line. Although the transitional region is too small, the process from fully laminar to fully turbulent boundary-layer flow is very regular, and the last velocity profile shown clearly obeys the law of the wall.

Hence, in the scope of the present study, it is not felt to be essential to cover the problem of transitional flow.

G. Final Result

According to the limiting N factor evaluated for the TWB wind tunnel, $N = 6$, and the computed N curves, Fig. 15, the transition location on the upper surface is evaluated at $X/C = 0.08$. On the lower surface, the N-factor values remain below the limiting N factor; hence, transition is imposed at the laminar separation point. The resulting values for the lift and drag coefficients for an angle of attack of $\alpha = 2$ deg are presented in Fig. 19, in addition to the measured data and the initial computed results with the adapted mesh, where transition is fixed at laminar separation. As can be seen, the lift is reduced slightly, due to the larger extent of the turbulent flow regime. However, the drag is nearly doubled and achieves a value within the range of the experimental data. Hence, the extent

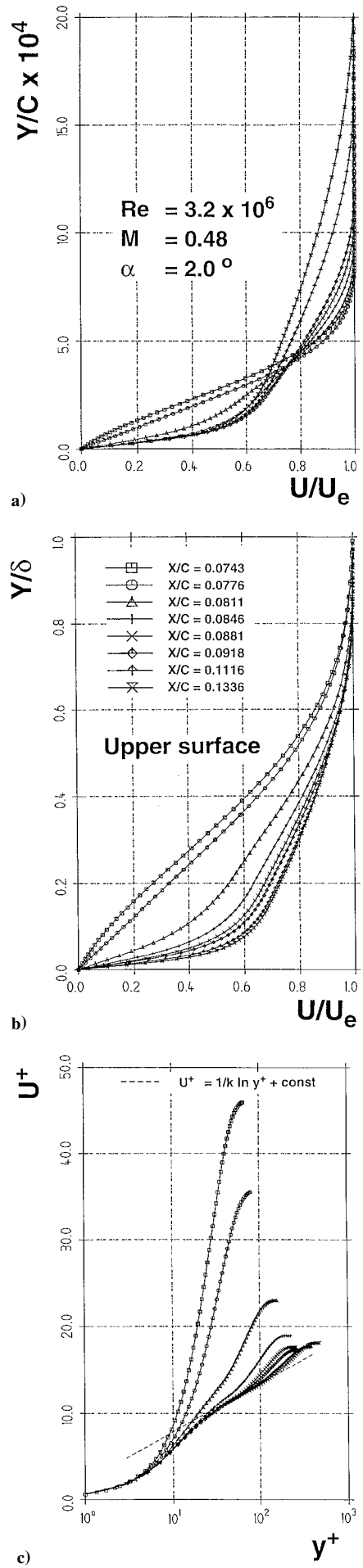

Fig. 18 Wall parallel velocity in the transitional flow region.

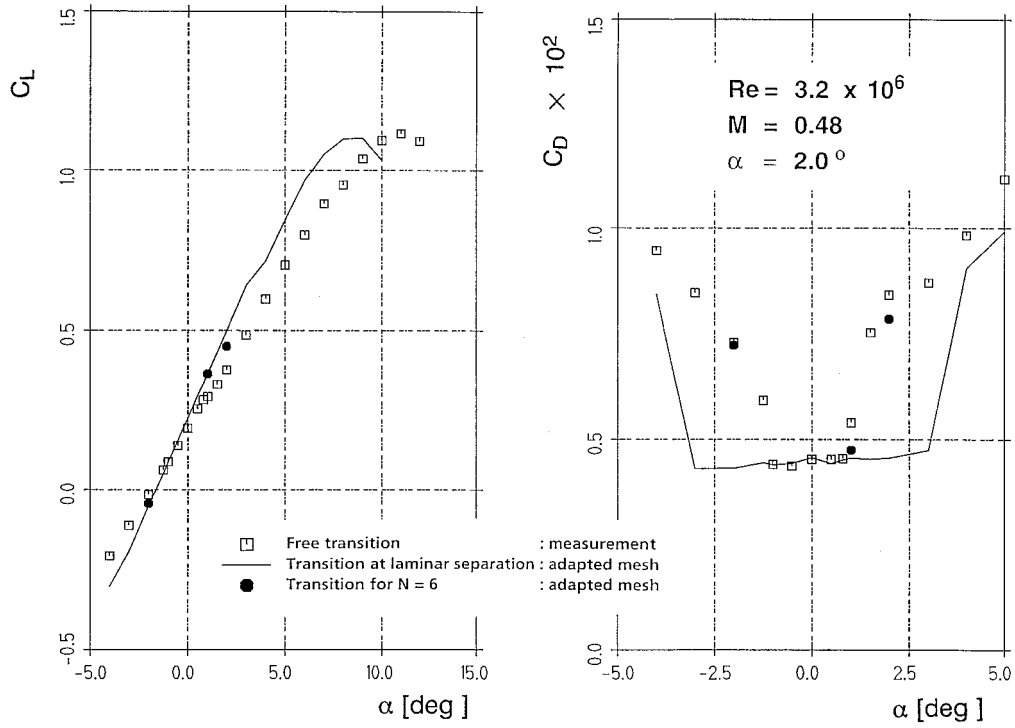

Fig. 19 Lift and drag polar for the DoAL3 airfoil including data with predicted transition location.

of the laminar bucket is clearly reduced and is now in agreement with the experimental findings.

To confirm the validity of the present approach, the procedure is repeated for angles of attack $\alpha = -2$ and 1 deg. The lift and drag data for the supplementary cases are shown in Fig. 19 and exhibit similar agreement with the experimental data.

IV. Performance Improvement

The main target of the present study is to show the feasibility of directly coupling the e^N method to the Navier–Stokes solver. The methods are applied sequentially, however, with considerable effort on the part of the user. The process can hardly be automated because most of the stability solvers do not automatically produce information about the unstable waves.

On the other hand, the actual results seem to indicate that a less elaborate data production process is possible. The inviscid Navier–Stokes results appear to be only slightly dependent on whether the laminar viscous results are produced with a high level of accuracy or not. Consequently, the computations with adapted meshes may be omitted, and the laminar viscous results do not have to be furnished by the Navier–Stokes method but rather via the use of a boundary-layer method. Hence, the iterative procedure now involves three computational methods: the Navier–Stokes, the boundary-layer, and the e^N methods. However, this approach will reduce the overall computational time and effort.

A further considerable reduction in engineering and computational effort is achievable if the stability solver of the e^N method is replaced by a database method.[12,13] In this case, the unstable frequencies and amplification rates are evaluated via table lookup, based on the viscous data. The major advantage is that the complete computational process, i.e., the iterative cycle of the Navier–Stokes, the boundary-layer, and the e^N database method, can now be automated. The Navier–Stokes solutions at a certain convergence level are then stopped, the boundary-layer and stability data are calculated without any further engineering input, the new transition locations are evaluated, and the Navier–Stokes solution is continued. Additionally, the cost of the database lookup procedure is significantly lower than the cost of the e^N stability solver.

V. Conclusions

A procedure is outlined that allows the user to determine from Navier–Stokes computations the a priori unknown length scales in the laminar as well as in the turbulent flow regimes. Based on the knowledge of the viscous layer thickness, a mesh adaption is performed, such that a sufficiently large and constant number of mesh points is embedded inside the viscous layer. It is shown via comparison with data from a boundary-layer method that the Navier–Stokes method produces laminar data of sufficient accuracy only with an appropiately adapted mesh.

As a benchmark case, the DoAL3 airfoil is used. The measured values of lift and drag are compared to computations with the initial and the adapted mesh first by imposing transition at the location of laminar separation. The maximum lift and the minimum drag are fairly well predicted. The value of $dc_L/d\alpha$ is overpredicted because the test section of the wind tunnel has slotted walls and the porosity may be too high. Most important, the extent of the laminar bucket is overpredicted because the laminar flow region is overestimated when imposing transition at laminar separation.

For angles of attack of $\alpha = -2$, 1, and 2 deg, transition on upper and lower surfaces is predicted via the e^N method and the knowledge of the limiting N factor of the wind tunnel. The lift is slightly reduced, due to the larger extent of turbulent flow. The computed drag doubles for $\alpha = -2$ and 2 deg, which is in good agreement with the experimentally observed values. The quality of the obtained results clearly demonstrates that the Navier–Stokes and the e^N methods for transition prediction can be coupled successfully to accurately compute the onset of transition.

Acknowledgment

This research has been supported in part by the European Commission in the BRITE/EURAM program EUROTRANS.

References

[1] Drela, M., and Giles, M. B., "Viscous–Inviscid Analysis of Transonic and Low Reynolds Number Airfoils," *AIAA Journal*, Vol. 25, No. 10, 1987, pp. 1347–1355.

[2] Stock, H. W., and Haase, W., "Determination of Length Scales in Algebraic Turbulence Models for Navier–Stokes Methods," *AIAA Journal*, Vol. 27, No. 1, 1989, pp. 5–14.

[3] Haase, W., "EUROVAL—A European Initiative on Validation of CFD Codes," *Notes on Numerical Fluid Mechanics*, Vol. 42, Vieweg–Verlag, Brunswick, Germany, 1992, pp. 82–87.

[4] Johnson, D. A., and King, L. S., "A Mathematical Simple Turbulence Closure Model for Attached and Separated Turbulent Boundary Layers," *AIAA Journal*, Vol. 23, No. 11, 1985, pp. 1684–1692.

[5]Horton, H. P., and Stock, H. W., "Computation of Compressible, Laminar Boundary Layers on Swept, Tapered Wings," *Journal of Aircraft*, Vol. 32, No. 6, 1995, pp. 1402–1405.

[6]Schrauf, G., "An Efficient Solver of the Eigenvalue Problem of the Linear Stability Equations for Three-Dimensional, Compressible Boundary Layer Flows," *6th DGLR-Fach-Symposium (Strömungen mit Ablösung)*, DLR, German Aerospace Center, DGLR-REP. 88-05, Bonn, 1988, pp. 18–27.

[7]Coles, D. E., "The Law of the Wake in the Turbulent Boundary Layer," *Journal of Fluid Mechanics*, Vol. 1, 1956, pp. 191–226.

[8]Horton, H. P., and Stock, H. W., "Near-Similarity Approximation for Compressible, Laminar Boundary Layers with Heat Transfer," *Journal of Aerospace Engineering* (submitted for publication).

[9]Müller, R., Puffert-Meißner, W., and Lück, H., "Messungen am Laminarprofil DoAL3 im Transsonischen Windkanal Braunschweig (TWB)," DLR-Interner Bericht, DLR, German Aerospace Research Establishment, Rept. IB 129-87/9, Brunswick, Germany, 1987.

[10]"Two-Dimensional Transonic Testing Methods," Final Report Garteur Action Group AD (AG-02), National Aerospace Lab. NLR, Rept. NLR TR 83086 L, Amsterdam, The Netherlands, 1981.

[11]Köster, H., and Müller, R., "Bestimmung des N-Faktors im Transsonischen Windkanal Braunschweig (TWB) anhand von Druckverteilungs- und Umschlagspunktmessungen und dem Sally-Verfahren," *6th DGLR-Fach-Symposium (Strömungen mit Ablösung)*, DLR, German Aerospace Center, DGLR-REP. 88-05, Bonn, 1988, pp. 66–77.

[12]Stock, H. W., and Degenhart, E., "A Simplified e^N-Method for Transition Prediction in Two-Dimensional, Incompressible Boundary Layers," *Zeitschrift für Flugwissenschaften und Weltraumforschung*, Vol. 13, No. 1, 1989, pp. 16–30.

[13]Stock, H. W., "The Stability and Amplification Rates of Two-Dimensional, Incompressible, Laminar Boundary Layers with Suction," *Zeitschrift für Flugwissenschaften und Weltraumforschung*, Vol. 14, No. 6, 1990, pp. 263–272.

P. Givi
Associate Editor